Fe-based amorphous coating with high corrosion and wear resistance

H. R. Ma, X. Y. Chen, J. W. Li, C. T. Chang, G. Wang, H. Li, X. M. Wang & R. W. Li

Published online: 10 May 2016.

Submit your article to this journal ⟲

Article views: 15

View related articles ⟲

View Crossmark data ⟲

Fe-based amorphous coating with high corrosion and wear resistance

H. R. Ma[1,2,3], X. Y. Chen[4], J. W. Li*[1,2], C. T. Chang*[1,2], G. Wang[3], H. Li[4], X. M. Wang[1,2] and R. W. Li[1,2]

The amorphous coating with a new developed composition of $Fe_{63}Cr_8Mo_{3.5}Ni_5P_{10}B_4C_4Si_{2.5}$ has been successfully prepared by high velocity oxygen fuel technique. The amorphous coating shows good corrosion and wear resistance, which compare favourably with those of the well-known SAM1651 ($Fe_{48}Mo_{14}Cr_{15}Y_2C_{15}B_6$) and SAM2X5 ($Fe_{49.7}Cr_{18}Mn_{1.9}Mo_{7.4}W_{1.6}B_{15.2}C_{3.8}Si_{2.4}$) amorphous coatings despite the absence of W, and very low Cr and Mo content. The electrochemical impedance spectroscopy (EIS) and Mott–Schottky analysis reveal that under high passive potentials the passive film on the coating reflects bi-layer structure and transpassive dissolution occurs, but the film can still remain passive due to slow ionic transport under these conditions. Donor densities of the passive films on the coatings are in the order of magnitude of 10^{21} cm^{-3} which is comparable to the reported values for passive films of SAM series amorphous coatings indicating the approximate stability of the passive film. In addition, the dominating wear mechanism of Fe-based amorphous coatings is oxidation wear.
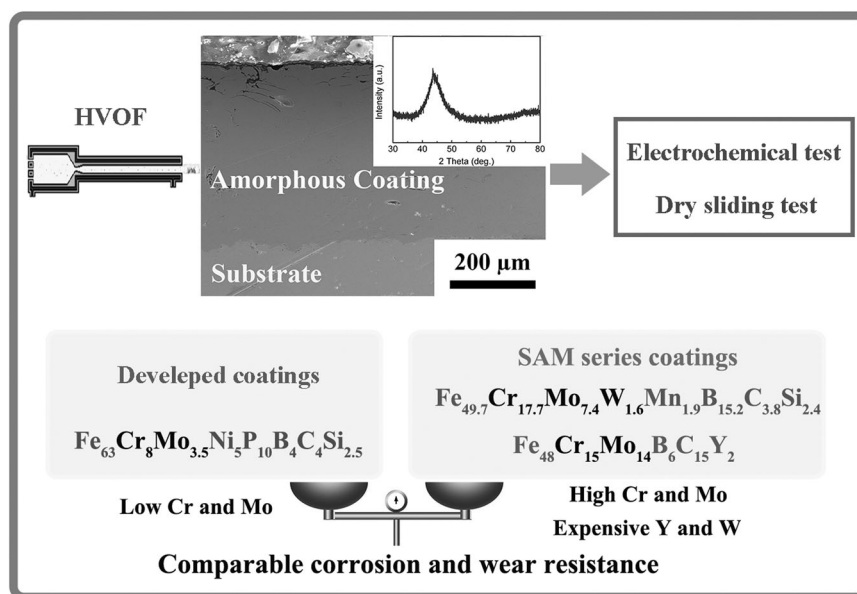
Keywords: Fe-based amorphous coating, Corrosion resistance, Wear resistance, Thermal spraying

[1]Key Laboratory of Magnetic Materials and Devices, Ningbo Institute of Materials Technology & Engineering, Chinese Academy of Sciences, Ningbo, Zhejiang 315201, China
[2]Zhejiang Province Key Laboratory of Magnetic Materials and Application Technology, Ningbo Institute of Materials Technology & Engineering, Chinese Academy of Sciences, Ningbo, Zhejiang 315201, China
[3]Laboratory for Microstructures, Shanghai University, Shanghai 200444, China
[4]Key Laboratory of Marine Materials and Related Technologies, Zhejiang Key Laboratory of Marine Materials and Protective Technologies, Ningbo Institute of Materials Technology and Engineering, Chinese Academy of Sciences, Ningbo, Zhejiang 315201, China

*Corresponding authors, email lijw@nimte.ac.cn (J. L.), ctchang@nimte.ac.cn (C. C.)

Introduction

Among the families of bulk metallic glasses (BMGs), Fe-based BMGs have attracted much attention because of their unique combination of outstanding properties including high strength and hardness, excellent corrosion and wear resistance, and good magnetic properties.[1–4] Unfortunately, the limited product size, poor plastic deformation and no work hardening at room temperature have seriously restricted the widespread applications of these materials.[5–7] Fe-based amorphous coatings as an

alternative form of Fe-based BMGs, can mitigate the drawbacks of these alloys, but carry forward the superiority in corrosion and wear resistance.[8–10]

The thermal spray processes with high cooling rates are suitable for obtaining amorphous coatings. Among various thermal spraying techniques, high velocity oxygen fuel (HVOF) process is superior to others due to the high kinetic energy process and relatively low flame temperature, which favours the formation of an amorphous structure with decreased porosity and oxide content.[11–19]

During the last decades, the compositions of SAM2X5 ($Fe_{49.7}Cr_{17.7}Mn_{1.9}Mo_{7.4}W_{1.6}B_{15.2}C_{3.8}Si_{2.4}$)[11–15] and SAM1651 ($Fe_{48}Mo_{14}Cr_{15}Y_2C_{15}B_6$)[11,16–19] have attracted special attention, which not only exhibit excellent corrosion resistance in aggressive environments, but also possess superior wear resistance. It is well-known that the additions of Mo, W and Cr can significantly improve the corrosion and wear resistance of Fe-based alloys,[20–23] thus the SAM series alloys usually contain high Mo and Cr as well as expensive W. However, these elements would increase the cost of raw materials required for the production of Fe-based amorphous coatings. To achieve cheap Fe-based amorphous metals without deteriorating the corrosion and wear resistance, we systematically studied the effect of minor Ni and P additions on the glass-forming ability and mechanical properties of SAM1651 alloy. It was found that the $Fe_{63}Cr_8Mo_{3.5}Ni_5P_{10}B_4C_4Si_{2.5}$ (at.-%) alloy prepared by industrial raw materials can be cast into cylinders with up to 3 mm in diameter, and exhibits high strength of 3300 MPa and plasticity of 0.9%.[24] In this work, the excellent corrosion and wear resistance of $Fe_{63}Cr_8Mo_{3.5}Ni_5P_{10}B_4C_4Si_{2.5}$ amorphous coating synthesised by HVOF is exposed. This work will enlighten further research on designing novel amorphous coatings with unique properties and expand the application of Fe-based amorphous coatings in engineering fields.

Experimental procedures

$Fe_{63}Cr_8Mo_{3.5}Ni_5P_{10}B_4C_4Si_{2.5}$ (at.-%) powders were produced by high pressure argon gas atomisation using industrial raw materials. Powders with dimension of 20–45 μm were sieved out as the feedstock powders. The mild steel was selected as substrate with a dimension of 20 mm × 20 mm × 3 mm. Prior to thermal spraying, all substrates were degreased by ethanol, dried in air, and then grit-blasted. The amorphous coatings were fabricated by HVOF thermal spray system in the open air. The detailed spraying parameters were given in Table 1.

The microstructures of the powders and as-sprayed coatings were characterised by scanning electron microscopy (SEM) (FEI Quanta FEG 250). Their phase structures were determined by X-ray diffraction (XRD) (D8 Advance) with Cu Kα radiation. The percentage porosity of the coatings were evaluated by analysing the SEM micrographs with the Image Pro-Plus 6.0 software. Thermal behaviour of the powders and corresponding coatings was investigated by differential scanning calorimeter (DSC) (NETZSCH 404C) in a flow of nitrogen atmosphere at a heating rate of 0.67 K s^{-1}.

Electrochemical measurements were conducted in 3.5 wt-% NaCl solution open to air at room temperature using an electrochemical workstation (Modulab, Solartron) with a three-electrode system. Platinum wire, saturated calomel electrode (SCE) and the coating were used as the counter electrode, reference electrode and working electrode, respectively. Prior to the test, all samples were polished to mirror finish, closely sealed with epoxy resin, leaving only an end-surface exposed for testing. Potentiodynamic polarisation was performed swept from −1 to 1.5 V at a potential sweep rate of 1.0 mV s^{-1}. For comparison, the melt-spun ribbon and mild steel were selected to perform the electrochemical measurements in the same way. EIS measurements were performed using a sinusoidal potential perturbation of 10 mV in a frequency range from 10 kHz to 0.01 Hz. Mott–Schottky (M–S) plots were determined by performing a potential scan toward the anodic direction to evaluate the semiconductor properties of the passive film. The measurement frequency in the M–S experiments was 1 kHz. The specimens for the EIS and M–S analysis were obtained by immersing them under the applied potentials (0.2, 0.4, 0.6 and 0.8 V) for 1800 s. Each test was repeated three to five times for repeatability and reliability.

Dry sliding tests were carried out with a ball-on-plate linear wear tester (UMT-3, Center for Tribology) at room temperature. Commercially available Al_2O_3 balls (manufacturer's nominal hardness 16.5 GPa; diameter = 9 mm) were used as the counterpart material. Before the wear test, all samples were polished to mirror finish. The parameters used are listed as follows: oscillating stroke of 7 mm, sliding speeds of 0.02 and 0.1 m s^{-1}, applied load of 20 N, and sliding distance of 250 m. New balls were used for each test. The wear volume loss and wear rate were calculated using the equation of $V = S \times d$ and $Q = (V/Nd_{total})$, where V is the wear volume (mm^3), S is the cross-sectional area (mm^2) of worn surfaces measured by a surface profile measuring instrument (Alpha-Step IQ), d means the oscillating stroke (mm), Q is the wear rate (mm^3 N^{-1} m^{-1}), N and d_{total} mean the applied load (N) and the total sliding distance (m), respectively. Each area value is the average of four measurements. The worn surfaces were characterised by SEM coupled with energy dispersive X-ray spectroscopy (EDX). For comparison, the mild steel was also selected to perform the tests in the same way. Hardness measurements were measured on the cross section of the coating and the mild steel using a Vickers hardness tester with an applied load of 9.8 N and a loading time of 15 s.

Results and discussion

Structures and morphology of the amorphous coatings

The morphology of the feedstock powders is shown in Fig. 1a. The majority of the particles produced by gas

Table 1 Spraying parameters employed in the HVOF process

Parameters	Condition
HVOF gun system	JP5000
Propane flow (L min^{-1})	35
Oxygen flow (L min^{-1})	25
Powder carrier gas flow (N$_2$, L min^{-1})	30
Feed rate (g min^{-1})	50
Spraying distance (mm)	300
Compressed air (MPa)	0.5
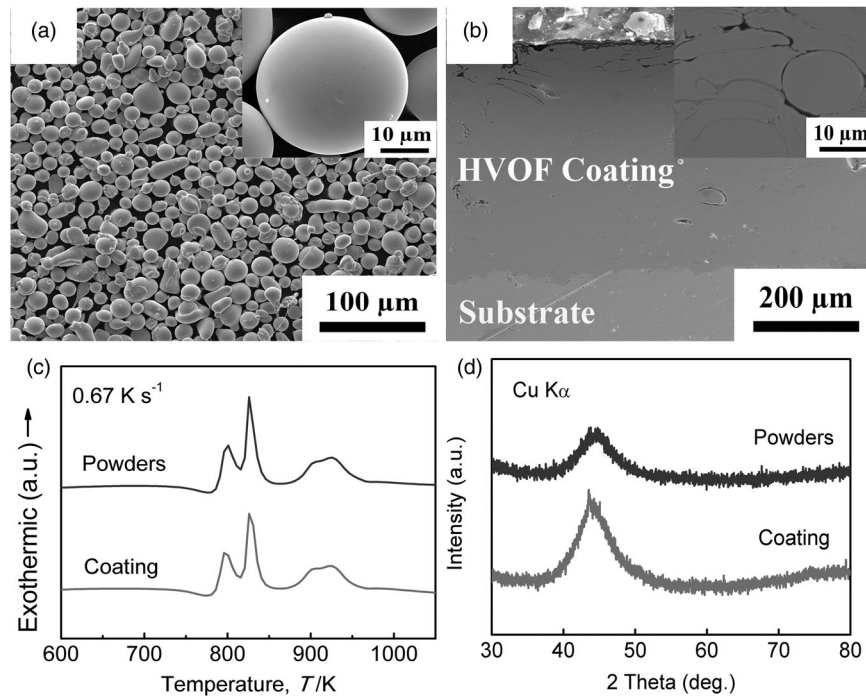
1 *a* SEM micrograph of the feedstock powders. The insert is the magnified image; *b* SEM micrograph of the HVOF-sprayed coating. The insert is the magnified image; *c* DSC traces and *d* XRD patterns of the HVOF-sprayed coating and the feedstock powders

atomisation are spherical or near-spherical with diameters of 20–45 μm and smooth surface, indicating the good fluidity of the powders. The typical cross-sectional morphology of the as-sprayed coating is displayed in Fig. 1*b*. The coating with thickness of around 300 μm adheres well to the substrate and has a dense structure with a porosity of less than 1.5%. The insert in Fig. 1*b* shows a magnified SEM image of the cross-sectional structure of the coating. There are some heterogeneous phases such as the unmelted particle and intersplat regions in the coating. Figure 1*c* and *d* presents the DSC curves and XRD patterns of the atomised powders and coating, respectively. No significant differences in thermal reaction behaviour between the DSC results of coating and powders can be observed, suggesting they may have similar content of amorphous phases. The coating shows an almost fully amorphous structure combined with a very tiny amount of crystalline content, while a broad halo without any distinguished sharp diffraction peaks indicates a complete amorphous

structure of the powders within the resolution limit of XRD.

Corrosion resistance of the amorphous coatings

Figure 2*a* shows the potentiodynamic polarisation curves of the amorphous coating with the corresponding amorphous ribbon and mild steel for comparison. The amorphous coating exhibits better corrosion resistance than the mild steel, while inferior to the fully amorphous ribbon due to the oxides, pores and microcracks distributed randomly in the coating. Table 2 summarises the corrosion current density (I_{corr}) and corrosion potential (E_{corr}) obtained for the studied coatings and SAM series coatings. It is observed that the corrosion resistance of $Fe_{63}Cr_8Mo_{3.5}Ni_5P_{10}B_4C_4Si_{2.5}$ coating compares favourably with that of the well-known SAM1651 and SAM2X5 amorphous coatings despite very low Cr and Mo content.[14,16] Figure 2*b* shows the SEM image of the corroded surface of the amorphous coating after
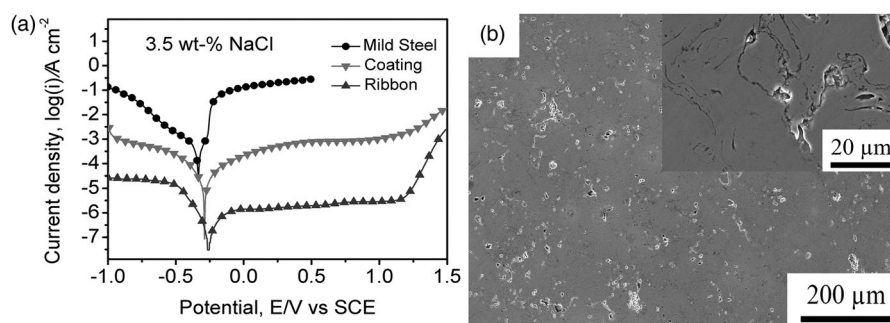
2 *a* Polarisation curve of the amorphous coating in comparison with the corresponding amorphous ribbon and mild steel; *b* SEM image of the corroded surface of the coating after potentiodynamic polarisation. The insert is the magnified image

Table 2 Summary of corrosion and wear properties of the amorphous coatings

Materials (at.-%)	Prepared methods	Corrosion properties		Wear properties				Refs.
		E_{corr}/V	I_{corr}/A cm^{-2}	Friction coefficient	Wear rate/mm^{3}N^{-1}m^{-1}	Contrast materials	Wear resistance	
$Fe_{63}C_{18}Mo_{3.5}Ni_5P_{10}B_4$ $C_4Si_{2.5}$ **(i)**	HVOF	−0.292	5.2×10^{-6}	0.6–0.7	$4–9 \times 10^{-5}$	Mild steel	5.24	Present
$Fe_{48}Mo_{14}Cr_{15}Y_2C_{15}B_6$ **(ii)**	HVOF	−0.305	2.3×10^{-6}	0.3–0.4	$3–19 \times 10^{-5}$	–	–	[16,17]
$Fe_{49.5}Cr_{17.8}Mo_{7.2}Mn_{1.8}W_{1.6}B_{15}C_{4.6}Si_{2.5}$	HVOF	−0.332	1.25×10^{-6}	–	–	–	–	[14]
$Fe_{49.7}Cr_{18}Mn_{1.9}Mo_{7.4}W_{1.6}B_{15.2}C_{3.8}Si_{2.4}$ **(iii)**	HVAF	–	–	0.75	Weight loss: 0.9 mg	Mild steel	4.67	[12]

The wear conditions: (i) test geometry: ball-on-plate, counter-face: Al$_2$O$_3$ ball (Φ 9.0 mm), sliding speed: 0.02–0.1 m s^{-1}, applied load: 10–20 N; (ii) test geometry: ball-on-plate, counter-face: Al$_2$O$_3$ ball (Φ 5.5 mm), sliding speed: 0.02–0.1 m s^{-1}, applied load: 16–32 N; (iii) test geometry: pin-on-disk, counter-face: 100Cr6 ball (Φ 12.0 mm), sliding speed of 0.4 m s^{-1}, applied load: 5 N.
The wear resistance is defined as wear rate/weight loss ratio of the contrast materials to that of those amorphous coatings

potentiodynamic polarisation. Localised corrosion attack can clearly be observed on the surface originated from pitting corrosion. The coating is preferentially corroded at defect sites, such as the oxidised boundary which would damage the uniformity of the passive film (the inset in Fig. 2b). This result is consistent with the pitting behaviour of the SAM1651 amorphous coating, where pitting occurs due to the galvanic effect between the Cr-depleted zone and Cr-rich intersplat region.[25]

Figure 3a shows the Nyquist plots of the amorphous coatings in 3.5 wt-% NaCl solution. The impedance at 0.2 V is the largest since the larger the formation potential, the greater the depression of the semi-circles. The insert is the corresponding Bode plots. Luo *et al.*[26] stated that this form of impedance indicated the occurrence of a charge-transfer reaction in a porous passive film. An equivalent circuit, $R_sR_1[Q_1(R_2Q_2)]$, is proposed to analyse the impedance data for the amorphous coatings, as shown in Fig. 3b.[26] R_s is the solution resistance; Q_1 represents the capacitance of the passive film, coupled with a resistance R_1 due to the ionic paths through the film; Q_2 represents the capacitance at the interfaces of electrolyte/passive film/metal; R_2 is the corresponding charge-transfer resistance. Figure 3c shows the applied potential dependence of the total resistance ($R_1 + R_2$) obtained from the equivalent circuit. The total resistance increases with the applied potentials ranging from 0.2 to 0.6 V and then decreases with the further increase of potential. The decline of the resistance might be attributed to the transpassive dissolution, leading to the decrease in the barrier effect of the passive film.

To better understand the structural characteristic of the passive film, Mott–Schottky (MS) analysis based on the measurement of electrode capacitance was carried out. Figure 3d shows the Mott–Schottky plots for the passive films. Each plot has a positive slope in region A, indicating that the passive films of the coatings show an n-type semiconducting behaviour. The n-type semiconductor behaviour could facilitate the permeation of aggressive anions (such as Cl$^-$) into the passive film and cause localised corrosion.[27] On the other hand, the electronic properties of the films change from n-type to p-type in region B, which is consistent with the trend of the total resistance (Fig. 3c). It seems that the transpassive dissolution of the present amorphous coatings should occur near 0.6 V. However, a steep rise in current can only be observed at above 1.2 V (Fig. 2a) suggesting the breakdown of the passive film. The results indicate that there is a range of potentials (region B) in which the film shows a p-type electronic behaviour (suggesting the initiation of transpassive dissolution), but the film can still remain passive due to slow ionic transport under these conditions.[28]

In region C, the passive films formed at 0.6 and 0.8 V change into n-type semiconducting behaviour again. It is known that the semiconducting behaviour of stainless steel and other Fe–Cr or Fe–Cr–Ni based alloys usually reflects the duplex character of the surface films, where the corrosion products of external layer are expected to contain both FeOOH and Fe$_2$O$_3$.[26]

Therefore, the transition of semiconducting behaviour in region C can be interpreted in terms of the capacitive contribution of the external layer containing Fe(III) oxides/hydroxides. The corrosion products of the external layer would inhibit the absorption of Cl$^-$ into the surface of internal layer and diffusion of transpassive products into the solution, reinforcing the barrier effect of the passive film.
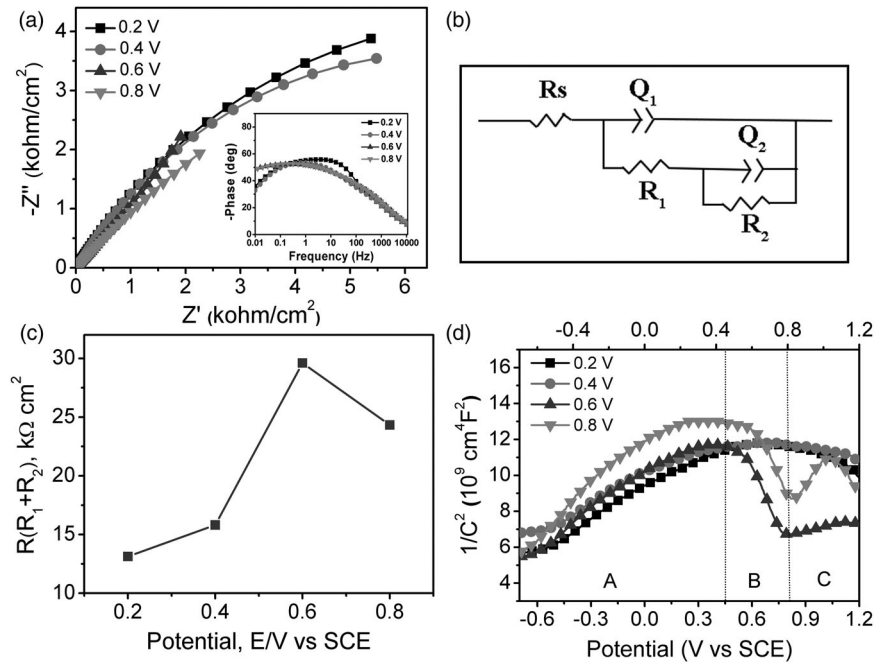
3 *a* Nyquist plots of the amorphous coatings at 0.2, 0.4, 0.6 and 0.8 V in 3.5 wt-% NaCl solution. The insert is the corresponding Bode phase plots; *b* equivalent circuit for describing impedance behaviour of the coatings; *c* total resistance for ion transfer ($R_1 + R_2$) as a function of the applied potential for the coatings; *d* Mott–Schottky plots of the passive films formed at 0.2, 0.4, 0.6 and 0.8 V
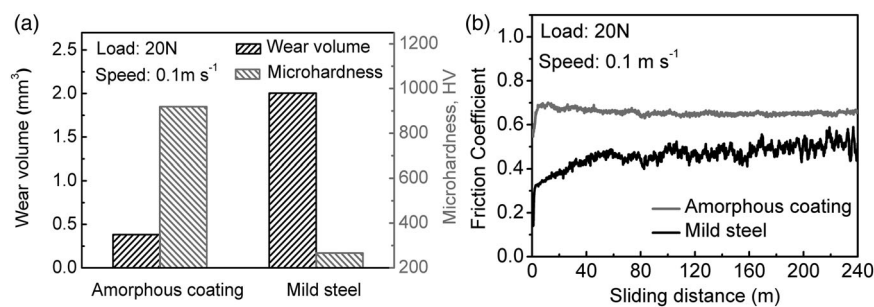
4 *a* Comparison of the wear volume and Vickers hardness of the amorphous coating and the mild steel; *b* friction coefficient curves of the amorphous coating and the mild steel as a function of sliding distance

According to the point defect model, the major carrier species in n-type oxide films are oxygen vacancies (donors) generated at the metal/oxide interface.[29,30] The donor density has a great influence on the stability of the passive films formed in chloride solutions. Higher donor densities lead to higher passive current densities. The calculated values of N_D (Donor density) are in the order of magnitude of 10^{21} cm^{-3} which is comparable and in similar range to the reported values for the passive film of SAM series amorphous coatings indicating the approximate stability of the passive film.[31] Detailed calculation method of N_D can be found in Wang *et al.*[31]

Wear behaviour of the amorphous coatings

The average wear volume loss after completion of sliding and the Vickers hardness of the test samples are showed in Fig. 4*a*. The average Vickers hardness of the coating is 920 HV, which is significantly higher than that of the mild steel. It also can be seen that the wear volume of the coating is approximately five times less than that of

the mild steel, indicating that the coating exhibits excellent wear resistance. Figure 4*b* shows the friction coefficient versus sliding distance curves of the amorphous coating and mild steel. The friction coefficient of the amorphous coating is more stable than that of the mild steel throughout the sliding test, implying that the former can keep slower wear loss for even much longer service time. Table 3 summarises the comparison of the wear resistance of various coatings. It is observed that the Fe$_{63}$Cr$_8$Mo$_{3.5}$Ni$_5$P$_{10}$B$_4$C$_4$Si$_{2.5}$ coating exhibits a prominent wear resistance, which compare favourably with that of the well-known SAM1651 and SAM2X5 amorphous coatings despite the absence of W, and very low Cr and Mo content,[12,17] making it an economic and effective candidate for protecting substrates withstanding frictional wear environment.

To understand the wear mechanism, the worn surfaces of the amorphous coatings at speeds of 0.02 and 0.1 m s^{-1} were further examined by SEM, as shown in Fig. 5. Table 3 shows the EDS analysis for sections A, B, C, D and E marked in Fig. 5. It can be seen in Fig. 5*a* that

Table 3 EDS results (at.-%) of the sections A, B, C, D and E in Fig. 5

Section	Fe	Cr	Mo	Ni	P	Si	O
A	54.25	7.73	3.99	4.29	12.12	3.10	14.52
B	36.77	4.81	2.39	2.71	7.48	1.72	44.12
C	21.74	3.13	1.22	1.71	4.10	0.96	67.14
D	41.03	5.11	2.44	3.56	8.16	2.06	37.64
E	27.58	1.44	0.57	0.92	2.34	0.73	66.42
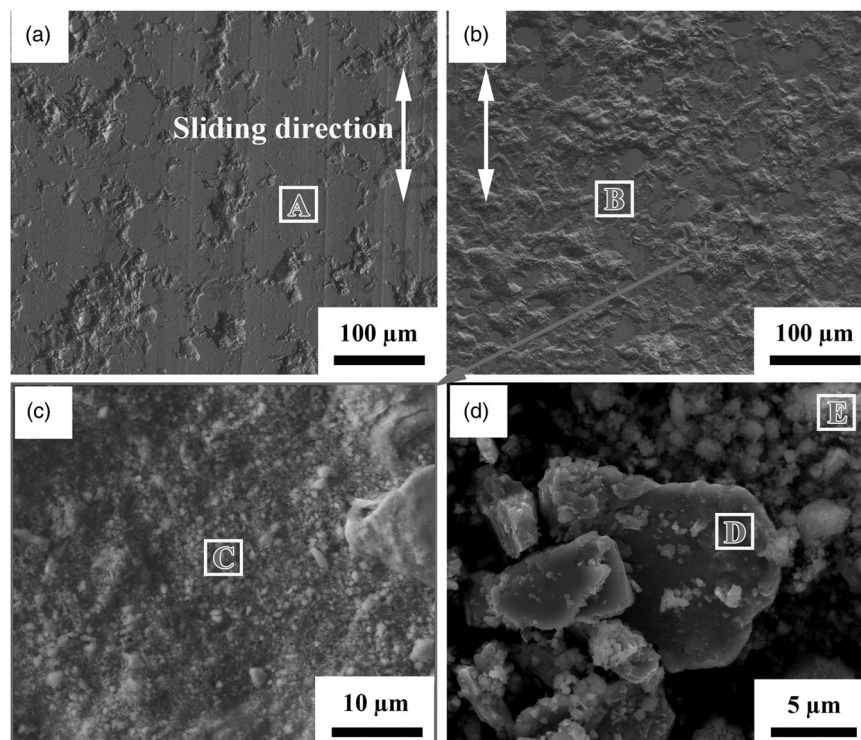
5 SEM images of the worn surfaces of the amorphous coatings at wear conditions: *a* 0.02 m s^{-1}, 20 N; *b* 0.1 m s^{-1}, 20 N. *c* Magnified SEM morphology from *b*; *d* SEM morphology of the worn-off debris

EDX analysis (section A) on the smooth part of the worn surface of the coating at low sliding speed shows signs of oxygen, implying that a smooth oxide tribolayer might form on the surface of the coating during the friction process. Figure 5*b* shows the worn surface of the amorphous coating at a fast sliding speed of 0.1 m s^{-1}. In contrast to the wear track at low sliding speed, the tribolayer formed at high sliding speed is rougher and more and wider wear pits can be observed, indicating that more material losses occur. For the case of section B, the content of oxygen dramatically increases to 44.12 at.-%. These results indicate that the oxidation of the coating surface at fast sliding speed is more serious. Figure 5*c* shows a magnified SEM image of the rough-contrast zone corresponding to the highly oxidised particles embedded in the worn pit. These particles imply that the abrasive particles dig into the sliding sample surface and then act as an accomplice to plow out material. The worn-off debris was also investigated, as shown in Fig. 5*d*. The large flakes (section D) with similar oxygen content compared to that of the smooth zone (section B) are thought to be peeled off from the amorphous coating surface. Zhang *et al.*[17] stated that the friction force can lead to the initiation of cracks at defect sites, such as pores and/or intersplat regions, resulting in flake-like splats delaminated from the amorphous

matrix. On the other hand, the small particles (section E) contain similar oxygen content compared with the worn pit (section C), much higher than that of the smooth zone (section B). The small highly oxidised particles may be generated from the oxide layer and perhaps from small metallic debris that might be removed and oxidised.

Based on the above experimental results and analyses, it is reasonable to deduce that one of the main wear mechanisms of the amorphous coating under dry sliding conditions is oxidation wear. The flash temperature under dry friction exceeds the glass transition temperature or the crystallisation temperature of the amorphous alloy, which leads to the serious oxidation of the coating surface.[32] The oxygen preferentially diffuses along the defective regions on the surface of coatings including pores, loose intersplats due to the high atomic activity of these regions. These oxides are usually brittle and prone to flaking off when the oxide layer grows to a critical thickness through continued flash friction heating, resulting in the increase of wear rate.

Conclusions

The amorphous coating with a new developed composition of $Fe_{63}Cr_8Mo_{3.5}Ni_5P_{10}B_4C_4Si_{2.5}$ has been

successfully prepared by HVOF technique. The corrosion and wear resistance of the amorphous coating compare favourably with those of the well-known SAM1651 (Fe$_{48}$Mo$_{14}$Cr$_{15}$Y$_2$C$_{15}$B$_6$) and SAM2X5 (Fe$_{49.7}$Cr$_{18}$Mn$_{1.9}$Mo$_{7.4}$W$_{1.6}$B$_{15.2}$C$_{3.8}$Si$_{2.4}$) amorphous coatings having enhanced corrosion and wear resistance despite the absence of W, and very low Cr and Mo content. The EIS and Mott–Schottky analysis reveal that under high passive potentials the passive film formed on the coating will reflects the duplex character and transpassive dissolution occurs, but the film can still remain pasive due to slow ionic transport under these conditions. Donor densities of the passive films on the coatings are in the order of magnitude of 10^{21} cm^{-3} which is comparable to the reported values for passive films of SAM series amorphous coatings indicating the approximate stability of the passive film. In addition, the dominating wear mechanism of the Fe-based amorphous coatings is oxidation wear. Based on the combination of good corrosion and wear resistance, the novel developed Fe-based amorphous coating is good candidate for applications in the areas involving high corrosion and wear.

Acknowledgements

References

1. A. L. Greer, K. L. Rutherford and M. Hutchings: 'Wear resistance of amorphous alloys and related materials', *Int. Mater. Rev.*, 2002, **47**, 87–112.
2. S. J. Pang, T. Zhang, K. Asami and A. Inoue: 'Synthesis of Fe–Cr–Mo–C–B–P bulk metallic glasses with high corrosion resistance', *Acta Mater.*, 2002, **50**, 489–497.
3. G. Herzer: 'Modern soft magnets: Amorphous and nanocrystalline materials', *Acta Mater.*, 2013, **61**, 718–734.
4. M. J. Shi, S. J. Pang and T. Zhang: 'Towards improved integrated properties in FeCrPCB bulk metallic glasses by Cr addition', *Intermetallics*, 2015, **61**, 16–20.
5. S. F. Guo, L. Liu, N. Lia and Y. Li: 'Fe-based bulk metallic glass matrix composite with large plasticity', *Scripta Mater.*, 2010, **62**, 329–332.
6. S. F. Guo, J. L. Qiu, P. Yu, S. H. Xie and W. Chen: 'Fe-based bulk metallic glasses: brittle or ductile?', *Appl. Phys. Lett.*, 2014, **105**, 161901.
7. X. B. Liang, J. B. Cheng, J. Y. Bai and B. S. Xu: 'Erosion properties of Fe based amorphous/nanocrystalline coatings prepared by wire arc spraying process', *Surf. Eng.*, 2010, **26**, 209–215.
8. S. Katakam, J. Y. Hwang, S. Paital, R. Banerjee, H. Vora and N. B. Dahatre: 'In situ laser synthesis of Fe-based amorphous matrix composite coating on structural steel', *Metall. Mater. Trans. A*, 2012, **43**, 4957–4966.
9. H. Zhang, Y. T. Xie, L. P. Huang, S. S. Huang, X. B. Zheng and G. Chen: 'Effect of feedstock particle sizes on wear resistance of plasma sprayed Fe-based amorphous coatings', *Surf. Coat. Technol.*, 2014, **258**, 495–502.
10. J. R. Lin, Z. H. Wang, P. H. Lin, J. B. Cheng, X. Zhang and S. Hong: 'Effect of crystallisation on electrochemical properties of arc sprayed FeNiCrBSiNbW coatings', *Surf. Eng.*, 2014, **30**, 683–687.
11. J. Farmer, J. S. Choi, C. Saw, J. Haslam, D. Day and P. Hailey: 'Iron-based amorphous metals: high-performance corrosion-resistant material development', *Metall. Mater. Trans. A*, 2009, **40**, 1289–1305.
12. R. Q. Guo, C. Zhang, Y. Yang, Y. Peng and L. Liu: 'Corrosion and wear resistance of a Fe-based amorphou s coating in underground environment', *Intermetallics*, 2012, **30**, 94–99.
13. W. H. Liu, F. S. Shieu and W. T. Hsiao: 'Enhancement of wear and corrosion resistance of iron-based hard coatings deposited by high-velocity oxygen fuel (HVOF) thermal spraying', *Surf. Coat. Technol.*, 2014, **249**, 24–41.
14. Z. B. Zheng, Y. G. Zheng, W. H. Sun and J. Q. Wang: 'Effect of applied potential on passivation and erosion–corrosion of a Fe-based amorphous metallic coating under slurry impingement', *Corros. Sci.*, 2014, **82**, 115–124.
15. S. D. Zhang, W. L. Zhang, S. G. Wang, X. J. Gu and J. Q. Wang: 'Characterisation of three-dimensional porosity in an Fe-based amorphous coating and its correlation with corrosion behaviour', *Corros. Sci.*, 2015, **93**, 211–221.
16. C. Zhang, R. Q. Guo, Y. Yang, Y. Wu and L. Liu: 'Influence of the size of spraying powders on the microstructure and corrosion resistance of Fe-based amorphous coating', *Electrochim. Acta*, 2011, **56**, 6380–6388.
17. C. Zhang, L. Liu, K. C. Chan, Q. Chen and C. Y. Tang: 'Wear behavior of HVOF-sprayed Fe-based amorphous coatings', *Intermetallics*, 2012, **29**, 80–85.
18. M. Yasir, C. Zhang, W. Wang, W. P. Xu and L. Liu: 'Wear behaviors of Fe-based amorphous composite coatings reinforced by Al$_2$O$_3$ particles in air and in NaCl solution', *Mater. Des.*, 2015, **88**, 207–213.
19. W. Wang, C. Zhang, P. Xu, M. Yasir and L. Liu: 'Enhancement of oxidation and wear resistance of Fe-based amorphous coatings by surface modification of feedstock powders', *Mater. Des.*, 2015, **73**, 35–41.
20. C. Scandian, C. Boher, J. D. B. de Mello and F. Rezai-Aria: 'Effect of molybdenum and chromium contents in sliding wear of high-chromium white cast iron: the relationship between microstructure and wear', *Wear*, 2009, **267**, 401–408.
21. J. Blink, J. Farmer, J. Choi and C. Saw: 'Applications in the nuclear industry for thermal spray amorphous metal and ceramic coatings', *Metall. Mater. Trans. A*, 2009, 40A, 1344–1354.
22. F. A. P. Fernandes, S. C. Heck, C. A. Picon, G. E. Totten and L. C. Casteletti: 'Wear and corrosion resistance of pack chromised carbon steel', *Surf. Eng.*, 2012, **28**, 313–317.
23. Y. Z. Lv, Y. F. Sun, J. Y. Zhao, G. W. Yu, J. J. Shen and S. M. Hu: 'Effect of tungsten on microstructure and properties of high chromium cast iron', *Mater. Des.*, 2012, **39**, 303–308.
24. J. W. Li, H. R. Ma, C. T. Chang, X. M. Wang and R. W. Li. "Synthesis and mechanical properties of FeCrMoNiPCBSi bulk metallic glasses" (Unpublished results).
25. C. Zhang, K. C. Chan, Y. Wu and L. Liu: 'Pitting initiation in Fe-based amorphous coatings', *Acta Mater.*, 2012, **60**, 4152–4159.
26. H. Luo, C. F. Dong, K. Xiao and X. G. Li: 'Characterization of passive film on 2205 duplex stainless steel in sodium thiosulphate solution', *Appl. Surf. Sci.*, 2011, **258**, 631–639.
27. S. Fujimoto and H. Tsuchiya: 'Semiconductor properties and protective role of passive films of iron base alloys', *Corros. Sci.*, 2007, **49**, 195–202.
28. M. A. Rodriguez and R. M. Carranza: 'Properties of the passive film on alloy 22 in chloride solutions obtained by electrochemical impedance', *J. Electrochem. Soc.*, 2011, **158**, C221–C230.
29. D. D. Macdonald: 'The point-defect model for the passive state', *J. Electrochem. Soc.*, 1992, **139**, 3434–3449.
30. D. D. Macdonald: 'On the existence of our metals-based civilization I. Phase-space analysis', *J. Electrochem. Soc.*, 2006, **153**, B213–B224.
31. Y. Wang, S. L. Jiang, Y. G. Zheng, W. Ke, W. H. Sun and J. Q. Wang: 'Effect of porosity sealing treatments on the corrosion resistance of high-velocity oxy-fuel (HVOF)-sprayed Fe-based amorphous metallic coatings', *Surf. Coat. Technol.*, 2011, **206**, 1307–1318.
32. J. Kong, D. S. Xiong, J. L. Li, Q. X. Yuan and R. Tyagi: 'Effect of flash temperature on tribological properties of bulk metallic glasses', *Tribol. Lett.*, 2009, **35**, 151–158.